Soil Dynamics and Earthquake Engineering 130 (2020) 105987

Contents lists available at ScienceDirect

Soil Dynamics and Earthquake Engineering

journal homepage: http://www.elsevier.com/locate/soildyn

Comparative investigation on optimal viscous damper placement for elastic-plastic MDOF structures: Transfer function amplitude or double impulse

Hiroki Akehashi, Izuru Takewaki *

Department of Architecture and Architectural Engineering, Graduate School of Engineering, Kyoto University, Kyotodaigaku-Katsura, Nishikyo, Kyoto, 615-8540, Japan

ARTICLE INFO

Keywords:
Critical excitation
Elastic-plastic earthquake response
Resonance
Viscous damper
Optimal damper placement
Double impulse
Transfer function amplitude

ABSTRACT

The effectiveness of the optimal viscous damper placement for elastic-plastic multi-degree-of-freedom (MDOF) structures under the critical double impulse is demonstrated through the comparison with the optimal damper placement for elastic MDOF structures designed with respect to transfer function amplitudes at natural frequencies. The method for optimal viscous damper placement was proposed for elastic-plastic MDOF structures subjected to the critical double impulse as a representative of near-fault ground motions in the previous paper [1]. The double impulse is composed of two impulses with opposite directions and the critical interval is determined by using the criterion on the maximum input energy. The critical timing of the second impulse was found to be the timing which requires the vanishing of the sum of the restoring force and the damping force in the first story. Three models with different story stiffness distributions of main structures are treated to demonstrate the effectiveness of the optimal viscous damper placement under the critical double impulse. The double impulse pushover (DIP) procedure proposed in the previous paper for determining the input velocity level of the critical double impulse is examined further in this paper. It is demonstrated that the optimal viscous damper placement for elastic-plastic MDOF structures under the critical double impulse is more effective for pulse-type recorded earthquake ground motions than the optimal damper placement designed with respect to transfer function amplitudes at natural frequencies because several higher modes arising in the elastic-plastic response under pulse-type recorded earthquake ground motions can be well controlled by the design for the double impulse.

1. Introduction

Viscous, visco-elastic and hysteretic dampers have been used as effective passive dampers installed at interstories. It is commonly understood that hysteretic dampers are effective in general for impulsive ground motions with short duration [2–6] and viscous dampers are useful for long-duration ground motions.

Recently, it is reported after devastating earthquakes that near-fault ground motions of impulsive type with short duration are apt to cause large damage to building structures. Although viscous dampers are not necessarily effective for near-fault ground motions, they have advantages to be able to reduce both displacement and acceleration. It seems, therefore, preferable that, when designing viscous dampers, they can reduce the earthquake response to small-to-moderate level ground motions and prevent excessive deformation to large level ground motions, such as long-period ground motions.

Many useful researches on optimal damper placement have been accumulated so far (see Refs. [7–9]). Takewaki [10] proposed an optimality criterion-based approach including an incremental inverse-problem formulation in which the transfer function amplitude in terms of the sum of the interstory drifts at the fundamental natural frequency is minimized under the constraint on total damper quantity. This approach has an advantage that the algorithm is simple and the obtained result is independent of input ground motions. Aydin [11] extended this approach to the transfer function amplitude in terms of the base shear at the fundamental natural frequency. Fujita et al. [12] developed an optimization method for minimizing the maximum interstory drift in the transfer function under a constant total damper quantity. Adachi et al. [13] explored a new practical optimal design scheme of oil dampers by determining their relief forces in terms of the

* Corresponding author.
E-mail address: takewaki@archi.kyoto-u.ac.jp (I. Takewaki).

https://doi.org/10.1016/j.soildyn.2019.105987
Received 10 September 2019; Accepted 24 November 2019

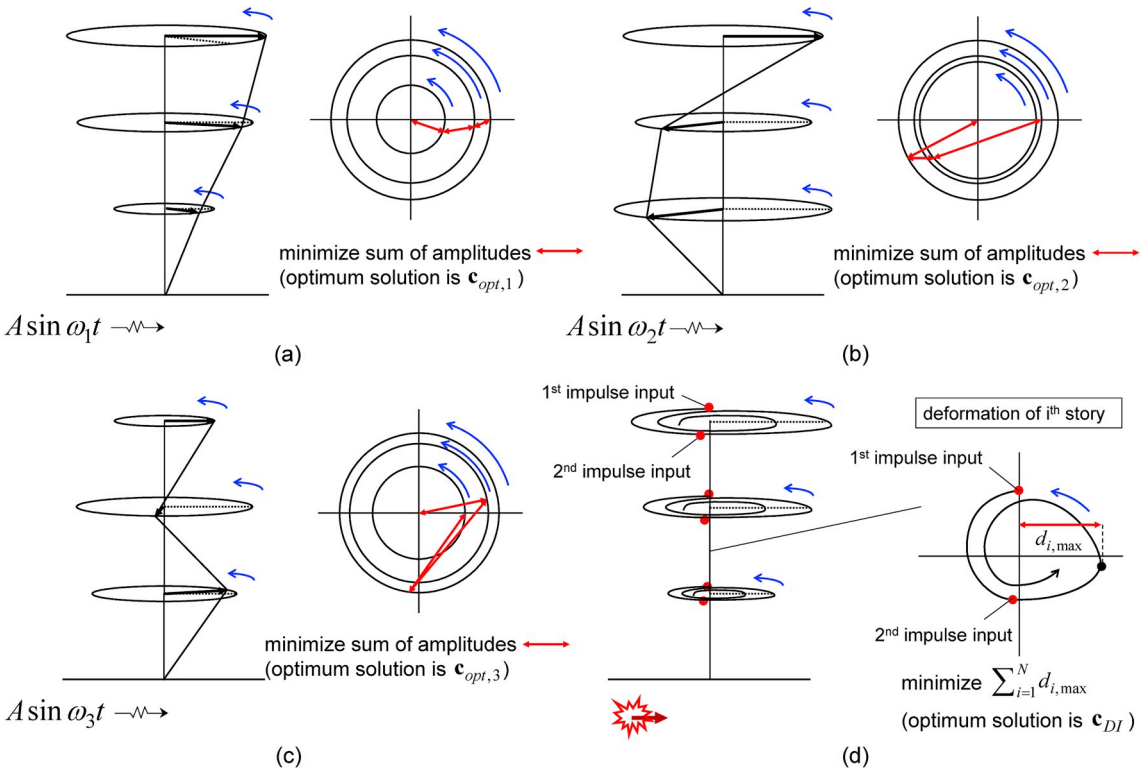

Fig. 1. Schematic diagram of criteria of optimal damper designs, (a) Transfer function amplitude at lowest natural frequency, (b) Transfer function amplitude at second natural frequency, (c) Transfer function amplitude at third natural frequency, (d) Sum of maximum interstory drifts under critical double impulse.

maximum interstory drift and the maximum top-story acceleration as the design targets. Lavan and Avishur [14] proposed an optimal viscous damper placement method under uncertain circumstances of structural and damper performances by using a Monte Carlo method. Some researches dealing with the comparison of several optimization techniques have also been conducted so far [15–18].

Since the objective of the introduction of passive dampers is to reduce the earthquake response of main structures to the elastic range, most of the research on optimal damper placement is limited to the elastic response. On the contrary, the research on the optimal damper placement for elastic-plastic structures is very limited, e.g. Refs. [1,14, 19–21]. It should be remarked that, even if an optimal damper placement is obtained for elastic structures, such placement is not necessarily optimal for elastic-plastic structures. This aspect is very important and interesting. In this paper, the detailed investigation will be presented on this issue.

In this paper, the effect of the distribution of passive dampers on elastic-plastic response of structures is investigated. By extending the approach of Takewaki [10] to higher-mode responses, the optimal passive damper placement for higher-mode responses will be proposed. Then such optimal dampers placement will be compared with the optimal damper placement for elastic-plastic structures under the critical double impulse [1] which was introduced by Kojima and Takewaki [22]. It is shown that the optimal damper placement for elastic-plastic structures under the critical double impulse is superior in the sense that such damper placement is effective for inputs with broader frequency range. For the optimal passive damper placements for each of (1–3)-mode responses and the optimal passive damper placement for elastic-plastic structures under the critical double impulse, the IDA procedure [23] and the DIP procedure [1] will be applied to investigate the elastic-plastic response characteristics of structures with various post-yield stiffness ratios.

2. Optimal damper placement with respect to transfer function amplitude at natural frequency and optimal damper placement under critical double impulse

2.1. Problem of optimal damper placement of elastic MDOF shear building structure with respect to transfer function amplitudes at natural frequencies

Consider a steady-state response of an N-story elastic MDOF shear building structure with viscous dampers at interstories under a harmonic excitation with frequency ω. Let $\mathbf{c}_{add}$, $\delta_l(\mathbf{c}_{add}, \omega)$ and ω_n denote the set of viscous dampers at interstories, the l-th steady-state interstory drift and the n-th natural circular frequency of the shear building structure. Following the method due to Takewaki [10], the transfer function amplitude at the fundamental natural circular frequency ω_1 can be defined as $f(\mathbf{c}_{add}, \omega_1) = \sum_{l=1}^{N} |\delta_l(\mathbf{c}_{add}, \omega_1)|$. This quantity indicates an approximate top-story displacement under a harmonic excitation with frequency ω_1. The first optimal design problem can be described by

$$\text{minimize } f(\mathbf{c}_{add}, \omega_1) = \sum_{l=1}^{N} |\delta_l(\mathbf{c}_{add}, \omega_1)| \text{subject to } \mathbf{c}_{add}^T \mathbf{1} = const. \quad (1)$$

where $\mathbf{1}$ is the vector with 1 at every component. This is the problem which was treated by Takewaki [10].

Consider next another optimal damper placement problem with respect to the transfer function amplitude at the second natural circular frequency ω_2.

$$\text{minimize } f(\mathbf{c}_{add}, \omega_2) = \sum_{l=1}^{N} |\delta_l(\mathbf{c}_{add}, \omega_2)| \text{subject to } \mathbf{c}_{add}^T \mathbf{1} = const. \quad (2)$$

This is a natural extension of the research due to Takewaki [10] into the second mode. The quantity $f(\mathbf{c}_{add}, \omega_2)$ indicates the sum of the interstory drifts under a harmonic excitation with frequency ω_2. To minimize $f(\mathbf{c}_{add}, \omega_2)$ is equal to averagely or approximately reducing the maximum interstory drift under such excitation. This treatment reflects the situation that, in high-rise buildings, long-period ground motions are

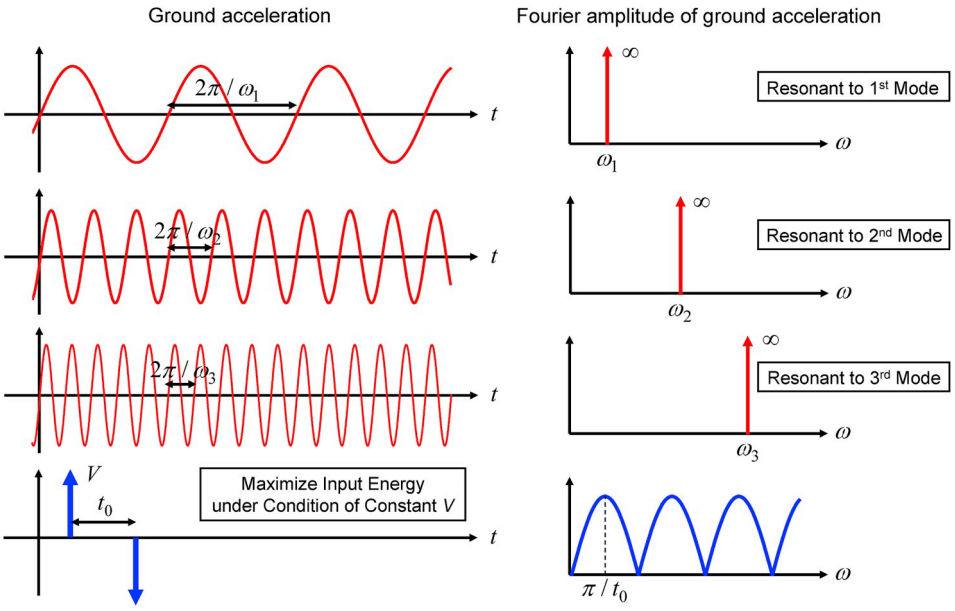

Fig. 2. Inputs used for respective optimal damper designs.

apt to be resonant to the second (or third) natural frequency of those buildings. Similarly, consider another optimal damper placement problem with respect to the transfer function amplitude at the third natural circular frequency ω_3.

$$\text{minimize } f(\mathbf{c}_{add},\ \omega_3)=\sum_{l=1}^{N}|\delta_l(\mathbf{c}_{add},\ \omega_3)| \text{ subject to } \mathbf{c}_{add}{}^T\mathbf{1}=const. \tag{3}$$

The quantity $f(\mathbf{c}_{add},\ \omega_3)$ indicates the sum of the interstory drifts under a harmonic excitation with frequency ω_3.

In this paper, the optimal damper placements with $f(\mathbf{c}_{add},\omega_n)$ as the objective function are called 'the n-th mode optimal damper placement' and are designated by $\mathbf{c}_{opt,\,1}$, $\mathbf{c}_{opt,\,2}$, $\mathbf{c}_{opt,\,3}$ for $n=1,\ 2,\ 3$. The optimal damper placement $\mathbf{c}_{opt,\,n}$ can be obtained by using the procedure presented by Takewaki [10] for $n=1$. The procedure due to Takewaki [10] adopts an optimality criterion-based approach including an incremental inverse-problem formulation in which the second-order differentiation of the transfer function is needed and an analytical expression can be used. The conceptual diagrams for the (1–3)-th mode optimal damper placements are shown in Fig. 1(a)-(c).

2.2. Optimal damper placement method for MDOF elastic-plastic shear building structures under critical double impulse

Akehashi and Takewaki [1] developed an effective optimal damper placement method for MDOF elastic-plastic shear building structures. Compared to the previous optimal damper placement methods for elastic-plastic structures, the method is efficient because the double impulse, given by $\ddot{u}_g(t)=V\delta(t)-V\delta(t-t_0)$, is an extremely simplified (but intrinsic-nature captured) input of near-fault ground motions and only a resonant critical case is treated. Here $\ddot{u}_g(t)$, V, t_0, $\delta(t)$ are the ground acceleration, the velocity amplitude, the interval of two impulses and the Dirac delta function. The critical timing of the second impulse is characterized by the criterion on the maximum input energy to the structure. For later comparison with the above-mentioned n-th mode optimal damper placement, the problem is stated below compactly.

Let $d_{\max,\,i}$ denote the maximum i-th interstory drift of the N-story elastic-plastic shear building structure with viscous dampers under the critical double impulse of the fixed velocity amplitude V and variable interval t_0 of two impulses satisfying the criticality condition. The optimal damper placement problem can be expressed by

$$\text{minimize} \sum_{i=1}^{N} d_{\max,\,i} \ \text{ subject to } \mathbf{c}_{add}^T\mathbf{1}=const. \tag{4}$$

The optimal damper placement for this problem is denoted by $\mathbf{c}_{DI}$. The conceptual diagram for the optimal damper placement for this problem is shown in Fig. 1(d). For better understanding, the inputs used for $\mathbf{c}_{opt,\,1}$, $\mathbf{c}_{opt,\,2}$, $\mathbf{c}_{opt,\,3}$, $\mathbf{c}_{DI}$ are presented in Fig. 2. It should be noted that, while the input resonant to the natural mode possesses the component $\omega=\omega_n$ only, the double impulse for $\mathbf{c}_{DI}$ has multiple components at wider frequency ranges. This property plays an important role in explaining the properties of $\mathbf{c}_{DI}$. It should also be reminded again that the interval t_0 of two impulses in the double impulse is varied for satisfying the criticality condition at every redesign step of dampers.

2.3. Amplification of higher-mode effect due to plastic response

It can be expected that plastic response induces complicated vibration components and higher modes are amplified. To investigate this phenomenon, the amplification of higher-mode effect due to plastic response is examined numerically.

Let $\mathbf{u}_n$ $(n=1,\ldots,N)$ denote the eigenmodes of the elastic model. Since an arbitrary vector of N-dimension can be expanded in terms of $\mathbf{u}_n$ $(n=1,\ldots,N)$, the velocity $\mathbf{V}(t)$ of floors can be expressed by

$$\mathbf{V}(t)=\sum_{n=1}^{N}\mathbf{u}_n\dot{q}_n(t) \tag{5}$$

where $\dot{q}_n(t)$ is the normal coordinate corresponding to $\mathbf{u}_n$. Let $\mathbf{M}$ denote the mass matrix. Premultiplication of $\mathbf{u}_m^T\mathbf{M}$ on both sides of Eq. (5) yields

$$\mathbf{u}_m^T\mathbf{M}\mathbf{V}(t)=\mathbf{u}_m^T\mathbf{M}\mathbf{u}_m\dot{q}_m(t) \ \Rightarrow\ \dot{q}_m(t)=\frac{\mathbf{u}_m^T\mathbf{M}\mathbf{V}(t)}{\mathbf{u}_m^T\mathbf{M}\mathbf{u}_m} \tag{6}$$

From Eq. (6), the m-th mode velocity response $\mathbf{u}_m\,\dot{q}_m(t)$ can be derived. This procedure can be applied not only to the elastic response, but also to elastic-plastic response. Furthermore, this procedure can also be applied to displacements and accelerations. Since the viscous damper allocation is dealt with in this paper, this procedure is applied to interstory velocities. It is noted that the importance of the maximum interstory velocities was pointed out by Adachi et al. [24] in the optimal viscous damper placement in high-rise buildings.

Fig. 3(a) shows 1, 5, 9, 12-th interstory velocities of the 12-story elastic shear building structure under Kobe Univ. NS during the

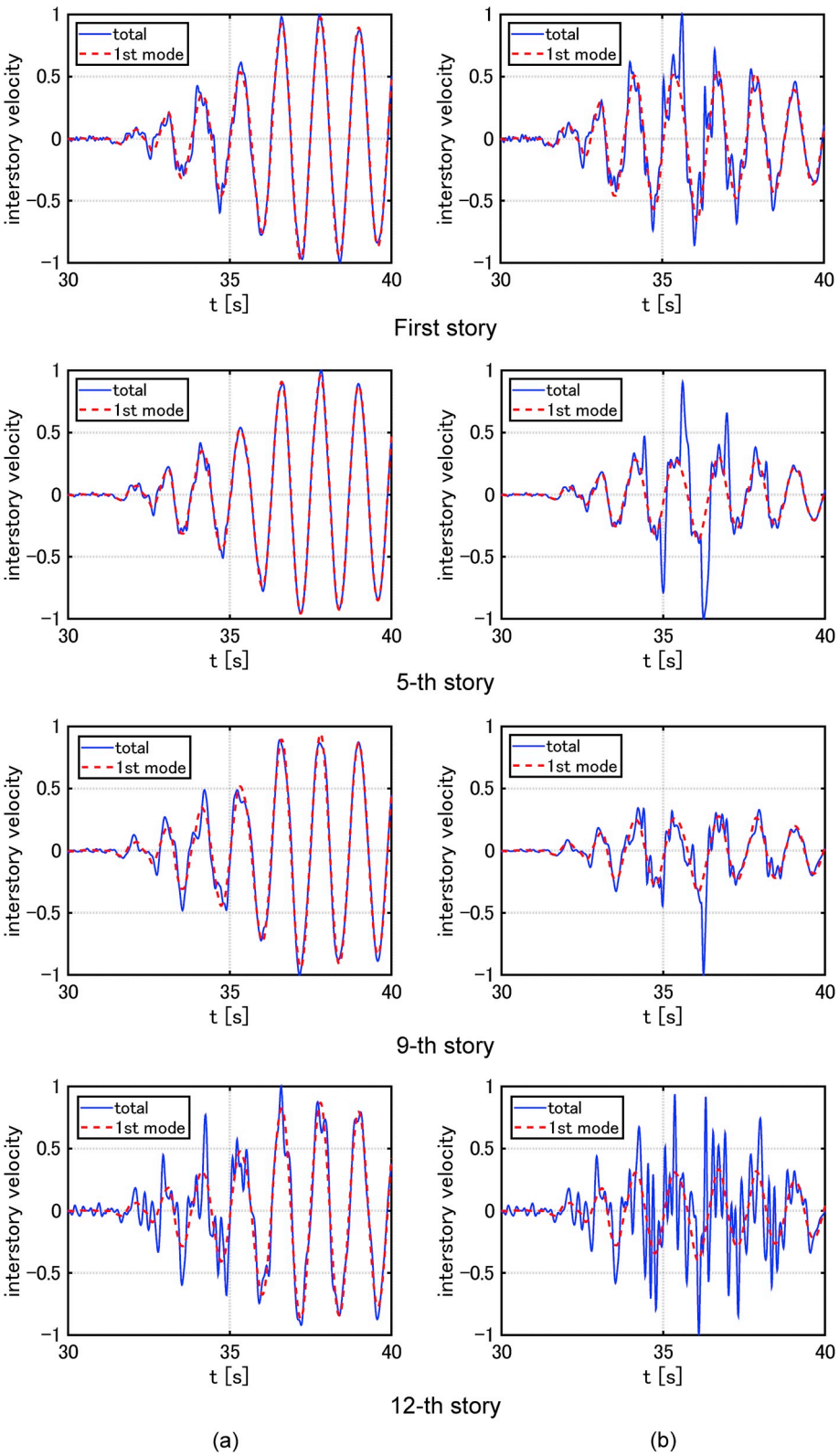

Fig. 3. Elastic eigenmode expansion of interstory velocity of elastic structure and elastic-plastic structure under Kobe Univ. NS (1995), (a) Elastic structure, (b) Elastic-plastic structure.

Hyogoken-Nanbu earthquake (1995). The story stiffness distribution is the stepped distribution (lower four stories, middle four stories and upper four stories have uniform stiffness distributions with different values/ the ratios among them are 2: 1.5: 1 from the bottom). This model corresponds to Model 3 in Ref. [1]. It can be observed that the first mode dominates the total response except the top story. On the other hand, Fig. 3(b) shows 1, 5, 9, 12-th interstory velocities of the 12-story elastic-plastic shear building structure under the same ground motion. The model has an elastic-perfectly plastic property. It can be seen that the ratio of the first mode (elastic model) decreases dramatically in the

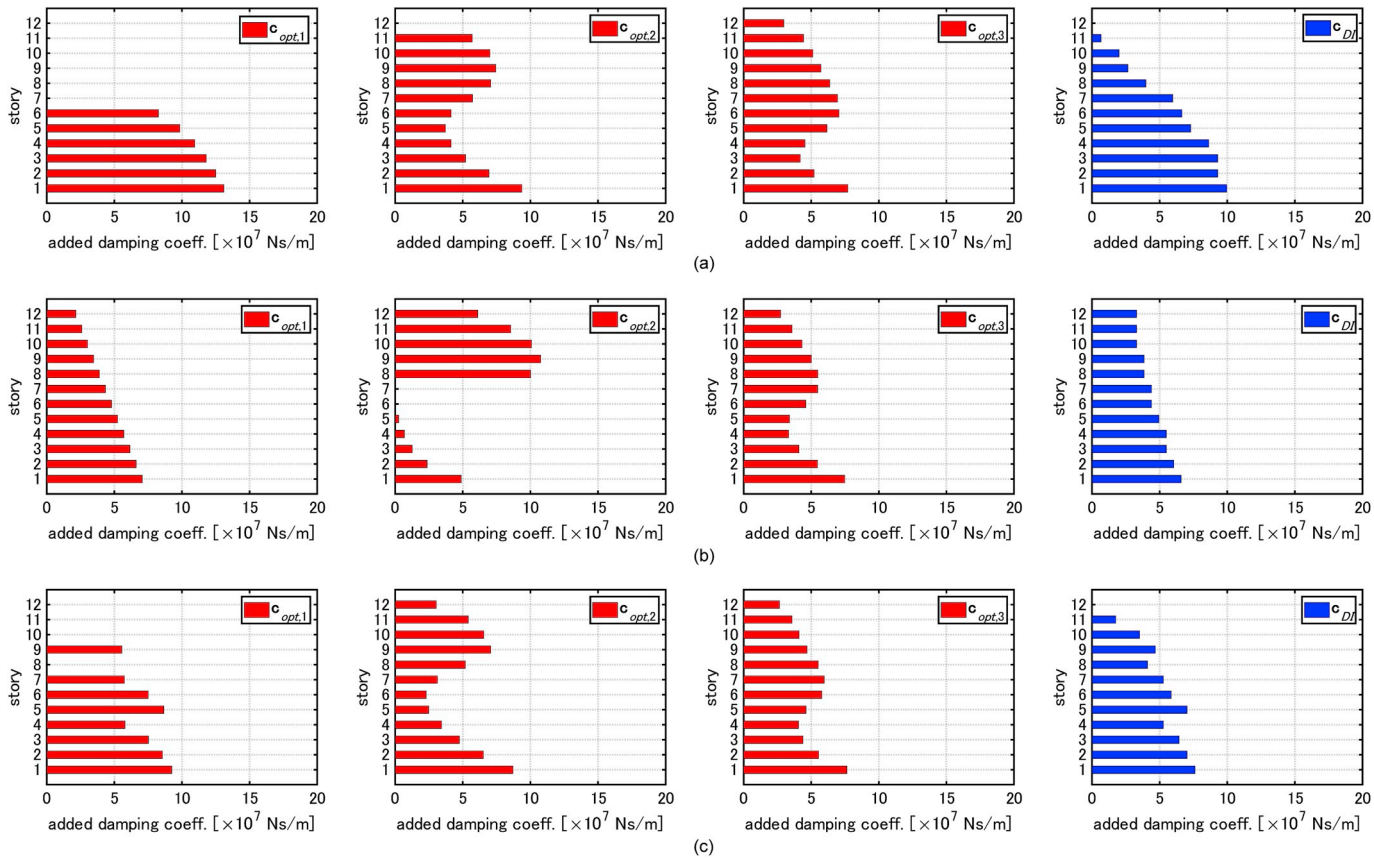

Fig. 4. Optimal damper distribution $\mathbf{c}_{opt,1}$, $\mathbf{c}_{opt,2}$, $\mathbf{c}_{opt,3}$, $\mathbf{c}_{DI}$, (a) Model 1 (Uniform story stiffness distribution), (b) Model 2 (Straight-line lowest eigenmode), (c) Model 3 (Uniform story stiffness distribution at every four stories).

elastic-plastic response.

2.4. Numerical examples of (1–3)-th mode optimal damper placement for elastic models and optimal damper placement for elastic-plastic models under critical double impulse

In this section, numerical examples of 12-story models are shown for the (1–3)-th mode optimal damper placements $\mathbf{c}_{opt,1}$, $\mathbf{c}_{opt,2}$, $\mathbf{c}_{opt,3}$ for elastic models and the optimal damper placement $\mathbf{c}_{DI}$ for elastic-plastic models under the critical double impulse.

Fig. 4 shows the optimal damper placements $\mathbf{c}_{opt,1}$, $\mathbf{c}_{opt,2}$, $\mathbf{c}_{opt,3}$, $\mathbf{c}_{DI}$ for Model 1 (Uniform story stiffness distribution), (b) Model 2 (Straight-line lowest eigenmode), (c) Model 3 (Uniform story stiffness distribution at every four stories, 1–4, 5–8, 9–12: stiffness ratio is 2: 1.5: 1 from the bottom). The fundamental natural period of all the models is 1.2[s]. The total damping coefficients of dampers are6.64, 5.50, 5.85 [$\times 10^8$Ns/m] for Models 1–3, respectively. These quantities correspond to the total damper quantities of the stiffness-proportional structural damping ratio 0.2.

In $\mathbf{c}_{opt,1}$, damping coefficients are concentrated to lower stories and there exist several stories without damper depending on stiffness models. In $\mathbf{c}_{opt,2}$, a large amount of dampers is concentrated to lower and upper stories. Similarly, in $\mathbf{c}_{opt,3}$, a large amount of dampers is concentrated to lower and middle stories. On the other hand, in $\mathbf{c}_{DI}$, dampers are allocated approximately to all stories. Furthermore, $\mathbf{c}_{opt,1}$ and $\mathbf{c}_{DI}$ are similar in Model 2.

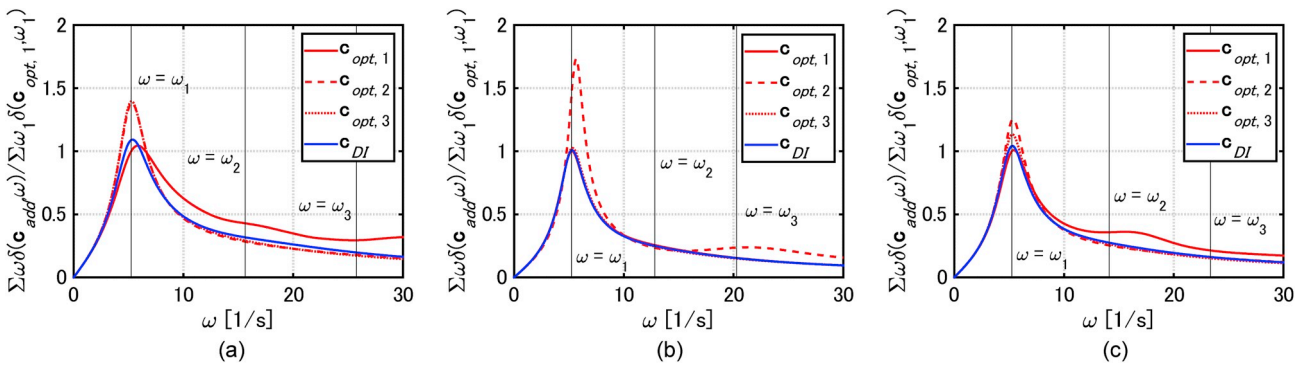

Fig. 5. Sum of transfer functions of interstory velocity $\sum_{l=1}^{N}\omega|\delta_l(\mathbf{c}_{add},\ \omega)|/\sum_{l=1}^{N}\omega_1|\delta_l(\mathbf{c}_{opt,1},\ \omega_1)|$ normalized for 1-st mode optimal design model, (a) Model 1, (b) Model 2, (c) Model 3.

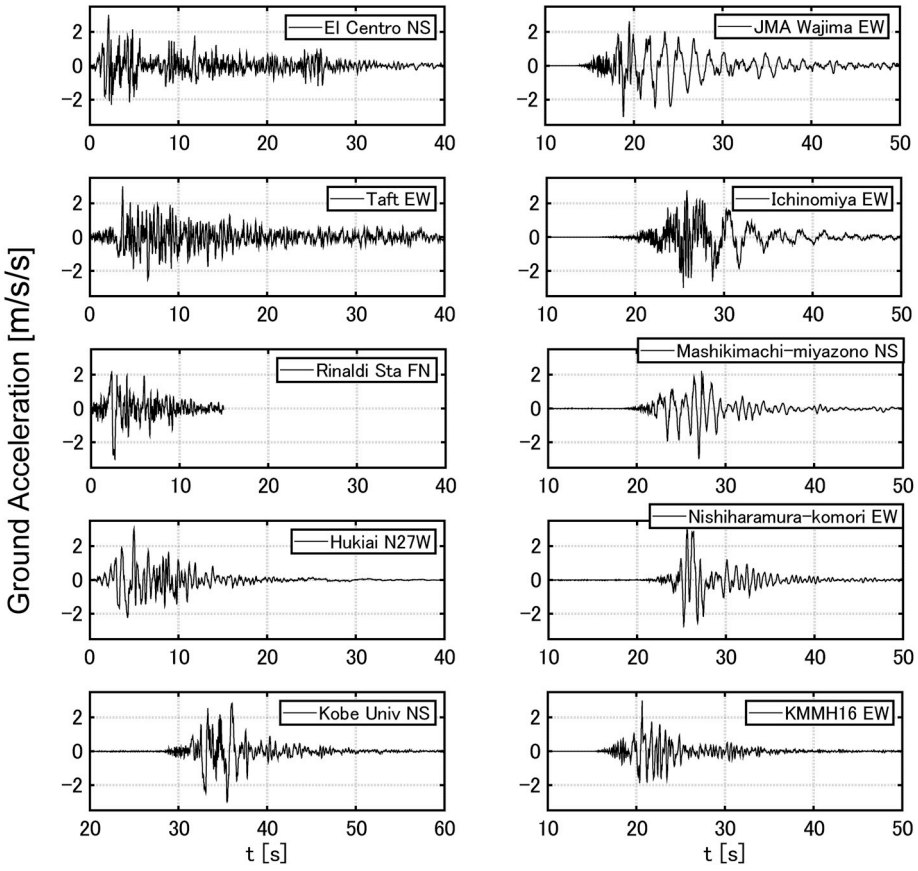

Fig. 6. Earthquake ground motions adopted for IDA.

2.5. Response control performance of damper placements optimally designed for various criteria

To investigate the response control performance of damper placements optimally designed for various criteria, the sum of the transfer functions of interstory velocity normalized for the 1-st mode optimal design model is evaluated. The sum of the transfer functions of interstory velocity can be expressed by

$$\omega f(\mathbf{c}_{add},\ \omega) = \sum_{l=1}^{N} \omega |\delta_l(\mathbf{c}_{add},\ \omega)| \tag{7}$$

Fig. 5 shows $\omega f(\mathbf{c}_{add},\ \omega)/\omega_1 f(\mathbf{c}_{opt,1},\ \omega_1)$ for Model 1–3. The optimal damper placements $\mathbf{c}_{opt,\,1}$, $\mathbf{c}_{opt,\,2}$, $\mathbf{c}_{opt,\,3}$, $\mathbf{c}_{DI}$ are substituted into $\mathbf{c}_{add}$.

The quantity $\omega f(\mathbf{c}_{add},\ \omega)$ at $\omega = \omega_1,\ \omega_2,\ \omega_3$ indicates the sum of the transfer function amplitudes of interstory velocity subjected to the sinusoidal inputs $\ddot{u}_g = \sin\omega_1 t,\ \sin\omega_2 t,\ \sin\omega_3 t$ resonant to the (1–3)-th natural circular frequencies or the sum of the transfer function amplitudes of interstory drift subjected to the sinusoidal inputs $\ddot{u}_g = \sin\omega_1 t,\ (\omega_2/\omega_1)\sin\omega_2 t,\ (\omega_3/\omega_1)\sin\omega_3 t$ with the same peak ground velocity and resonant to the (1–3)-th natural circular frequencies.

It can be said that, if $\omega f(\mathbf{c}_{add},\ \omega)$ is smaller in a wider frequency range, the corresponding damper placement possesses a higher response control performance. It can be observed from Fig. 5 that $\mathbf{c}_{opt,\,n}$ is not necessarily effective to other natural frequencies. On the other hand, $\mathbf{c}_{DI}$ exhibits a better response control performance. This may result from the fact that the double impulse has multiple frequency components as shown in Fig. 2 and $\mathbf{c}_{DI}$ is designed for such excitation.

It may be said that the comparison in the transfer function of interstory velocity indicates the comparison of $\mathbf{c}_{opt,\,1}$, $\mathbf{c}_{opt,\,2}$, $\mathbf{c}_{opt,\,3}$, $\mathbf{c}_{DI}$ in the elastic range for long-period ground motions. The performance comparison of $\mathbf{c}_{opt,\,1}$, $\mathbf{c}_{opt,\,2}$, $\mathbf{c}_{opt,\,3}$, $\mathbf{c}_{DI}$ in the elastic-plastic range for pulse-type ground motions will be shown in the next section.

Table 1
Recorded ground motions used for IDA.

1.	Imperial Valley 1940 El Centro NS	6.	Notohanto 2007 JMA Wajima EW
2.	Kern County 1952 Taft EW	7.	Kumamoto 4/16/2016 Ichinomiya EW
3.	Northridge 1994 Rinaldi Sta FN	8.	Kumamoto 4/16/2016 Mashikimachi-miyazono NS
4.	Hyogoken-Nanbu 1995 Hukiai N27W	9.	Kumamoto 4/16/2016 Nishiharamura-komori EW
5.	Hyogoken-Nanbu 1995 Kobe Univ NS	10.	Kumamoto 4/16/2016 KMMH16 EW

2.6. Application of Incremental Dynamic Analysis (IDA) to model 1–3 with damper placements $\mathbf{c}_{opt,\,1}$, $\mathbf{c}_{opt,\,2}$, $\mathbf{c}_{opt,\,3}$ $\mathbf{c}_{DI}$

Incremental Dynamic Analysis (IDA) was proposed by Vamvatsikos and Cornell [23] to demonstrate the sequential characteristics of the elastic-plastic response for increasing level of earthquake ground motions. In this section, IDA is applied to Model 1–3 with the optimal damper placements $\mathbf{c}_{opt,\,1}$, $\mathbf{c}_{opt,\,2}$, $\mathbf{c}_{opt,\,3}$, $\mathbf{c}_{DI}$. The stiffness-proportional damping of damping ratio 0.01 is assumed as structural damping.

The adopted earthquake ground motions and their numbers for IDA are indicated in Fig. 6 and Table 1. The corresponding velocity response spectra of damping ratio 0.05 for the adopted earthquake ground motions normalized to PGA 3.0 [m/s^2] are shown in Fig. 7 (two figures are provided for clarity). El Centro NS (1940) and Taft EW (1952) are representative ground motions of random nature. Rinaldi Station FN (1994), Fukiai N27W (1995), Kobe Univ. NS (1995) and JMA Wajima EW (2007) are representative ground motions of pulse type. Ichinomiya EW (2016), Mashikimachi-miyazono NS (2016), Nishiharamura-komori EW (2016) and KMMH16 EW (2016) are also representative ground motions of pulse type. The ground motions of pulse type have different

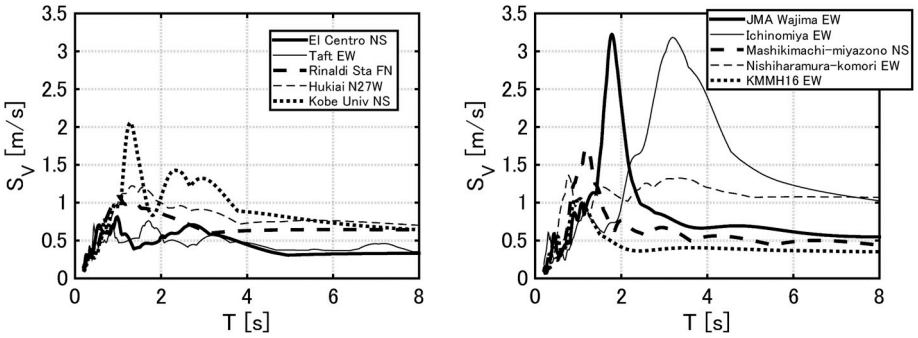

Fig. 7. Velocity response spectra for damping ratio $h = 0.05$ of recorded ground motions normalized by PGA = 3 [m/s^2] and used for IDA procedure.

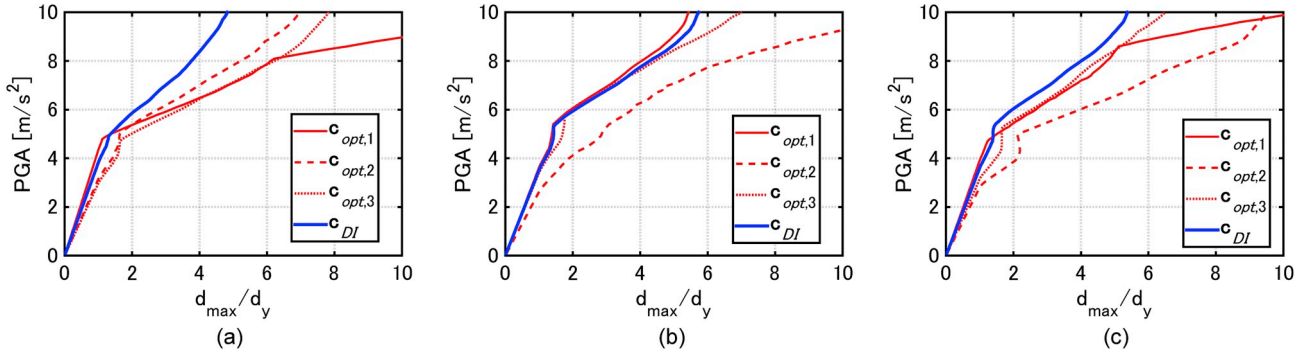

Fig. 8. Application of IDA: Maximum interstory drift with respect to peak ground acceleration, (a) Model 1, (b) Model 2, (c) Model 3.

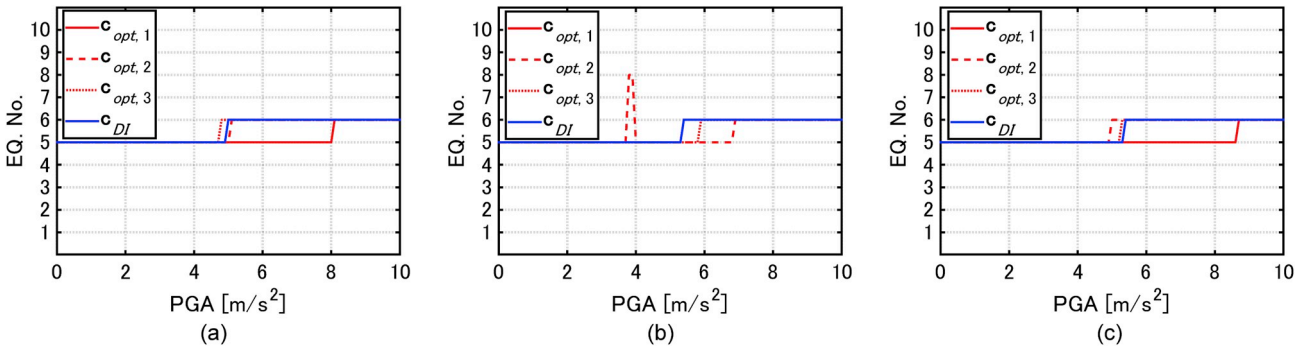

Fig. 9. Critical earthquake ground motion numbers for IDA, (a) Model 1, (b) Model 2, (c) Model 3.

characteristic periods as observed from Fig. 7. Since it is understood that viscous dampers are not necessarily effective for pulse-type ground motions, those ground motions were adopted to compare the performance. When long-period ground motions are taken into account, multi-impulse [25] can be treated as a representative input. However, in such a case, the definition of the critical input may be arguable for MDOF elastic-plastic structures. Such complicated problem may be discussed in the future.

Fig. 8 shows the plots of IDA for Model 1–3 with the optimal damper placements $\mathbf{c}_{opt,1}$, $\mathbf{c}_{opt,2}$, $\mathbf{c}_{opt,3}$, $\mathbf{c}_{DI}$. From Fig. 8, the following observations can be drawn. The peak ground acceleration corresponding to $d_{\max}/d_y = 1$ (elastic limit) becomes the largest in the model of $\mathbf{c}_{opt,1}$. The peak ground acceleration corresponding to $d_{\max}/d_y = 1$ in the model of $\mathbf{c}_{DI}$ is also large and is almost equivalent to that in the model of $\mathbf{c}_{opt,1}$. As for the plastic deformation after yielding, the model of $\mathbf{c}_{opt,1}$ exhibits larger values than other models in some cases. On the other hand, the model of $\mathbf{c}_{DI}$ exhibits smaller plastic deformations. Also for the models of $\mathbf{c}_{opt,2}$ and $\mathbf{c}_{opt,3}$, the plastic deformation after yielding is apt to become larger. Fig. 9 illustrates the earthquake ground motion numbers which are critical in the application of IDA for Model 1–3 with the optimal damper placements $\mathbf{c}_{opt,1}$, $\mathbf{c}_{opt,2}$, $\mathbf{c}_{opt,3}$, $\mathbf{c}_{DI}$. It can be observed from Fig. 9 that Kobe Univ. NS in 1995 is critical in the lower range of PGA and JMA Wajima EW in 2007 is critical in the upper range of PGA for all models. It should be noted that the predominant period of the former earthquake is about 1.2 [s] and that of the latter is about 1.8 [s] as observed in Fig. 7. It seems that, as PGA becomes large and the plastic deformation level increases, the equivalent natural period is lengthened and the critical ground motion changes.

3. Plastic deformation characteristics of building structures with optimal damper locations for increasing level of critical double impulse

3.1. Double impulse pushover (DIP) and its significance

IDA was used in the previous section. Since IDA uses recorded ground motions, the results may provide realistic findings. However, the properties of recorded ground motions depend strongly on the level of

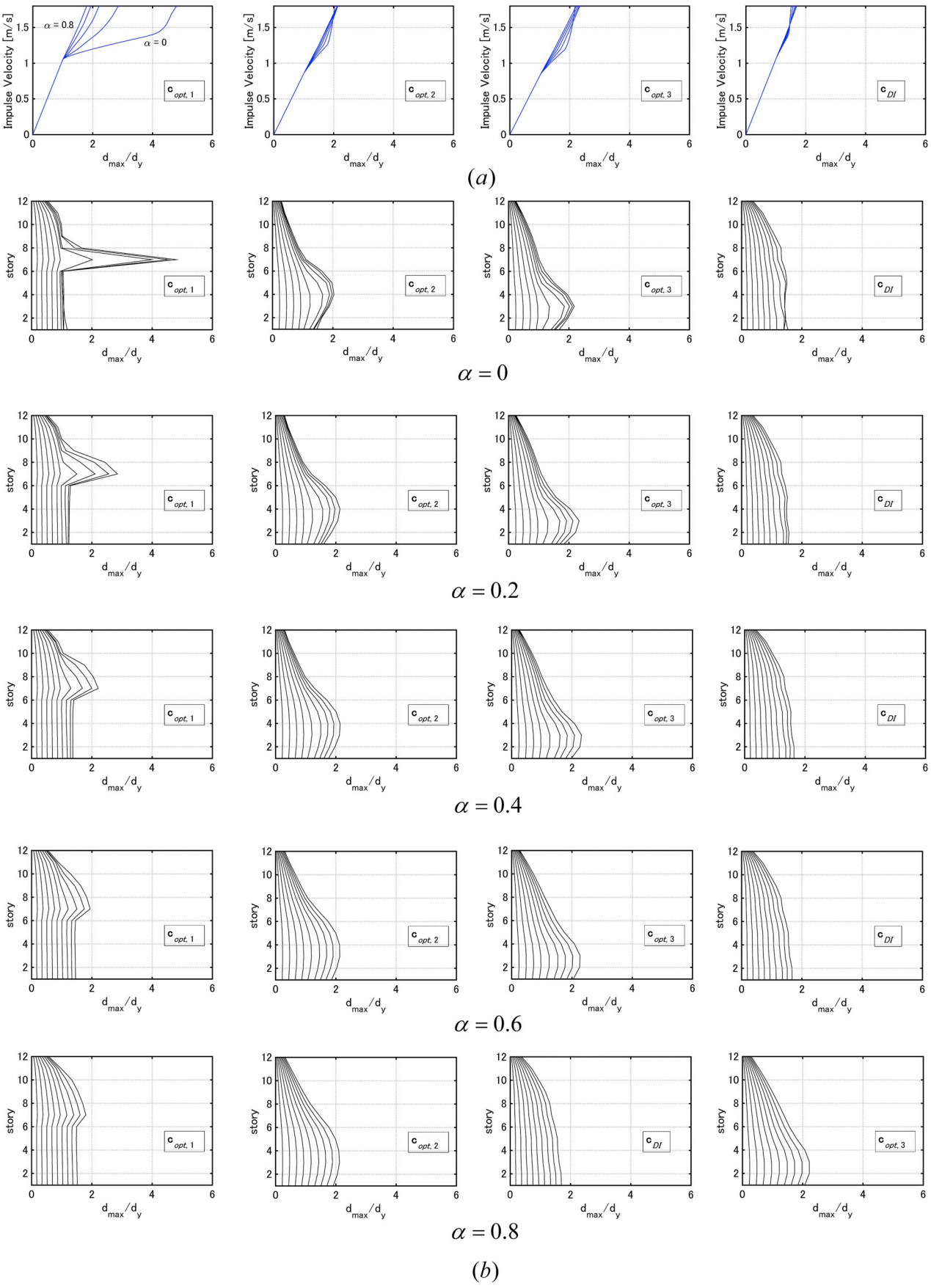

Fig. 10. DIP analysis for Model 1: Maximum interstory drift, (a) Maximum interstory drift with respect to input velocity level, (b) Maximum interstory drift for various input velocity levels $V = 0.2$–1.8 [m/s] and various second stiffness ratio after yielding.

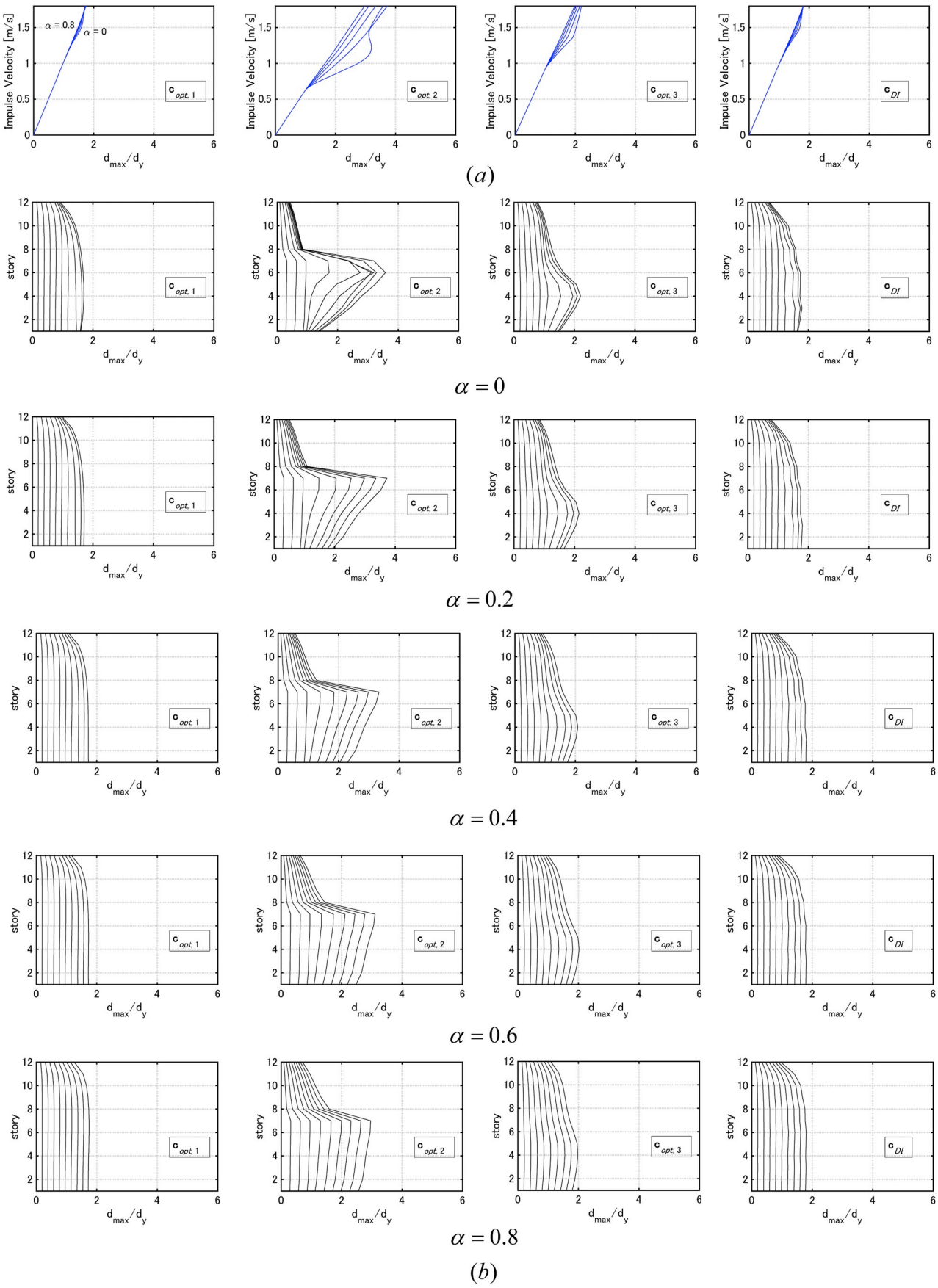

Fig. 11. DIP analysis for Model 2: Maximum interstory drift, (a) Maximum interstory drift with respect to input velocity level, (b) Maximum interstory drift for various input velocity levels $V = 0.2$–1.8 [m/s] and various second stiffness ratio after yielding.

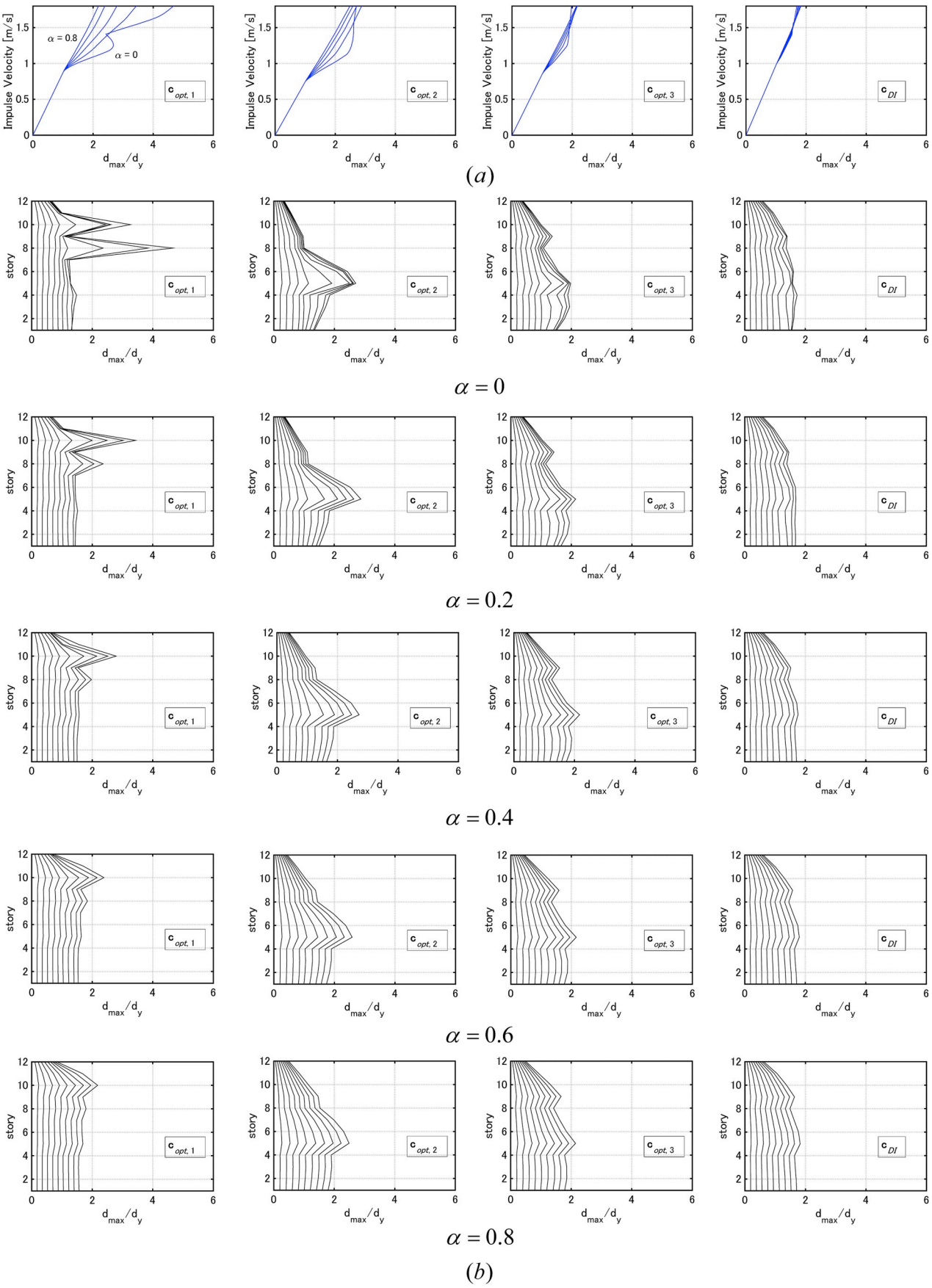

Fig. 12. DIP analysis for Model 3: Maximum interstory drift, (a) Maximum interstory drift with respect to input velocity level, (b) Maximum interstory drift for various input velocity levels $V = 0.2$–1.8 [m/s] and various second stiffness ratio after yielding.

earthquakes (magnitude etc.). For this reason, the simple level change conducted in IDA may cause some unrealistic results. Near-fault ground motions are recorded at various places recently and include pulse-type components. The level and characteristic period of such pulse-type ground motions exhibit various aspects. To respond to such uncertain and complicated occurrence of pulse-type ground motions, Akehashi and Takewaki [1] introduced a new concept of Double Impulse Pushover (DIP). In DIP, only the critical double impulse with the critical interval of two impulses resonant to elastic-plastic structures is dealt with. It is noted that the critical interval of two impulses resonant to elastic-plastic structures depends on the input velocity level. Then the input level of velocity is increased and the corresponding maximum elastic-plastic response is plotted. DIP has an advantage over the conventional IDA in the sense that DIP provides a stable relation between the input level and the maximum elastic-plastic response.

3.2. Numerical examples of application of DIP

DIP has been applied to Model 1–3 with the optimal damper placements $\mathbf{c}_{opt,1}$, $\mathbf{c}_{opt,2}$, $\mathbf{c}_{opt,3}$, $\mathbf{c}_{DI}$. Figs. 10–12 show the results of DIP for Model 1, 2 and 3, respectively. The plot (a) presents the relation of the maximum interstory drift with respect to the input velocity level. In addition, the plot (b) indicates the change of the distribution of the maximum interstory drift for varied input velocity level 0.2–1.8 [m/s]. In the plot (b), five models of second stiffness ratio after yielding $\alpha = 0$, 0.2, 0.4, 0.6, 0.8 are considered. The case of $\alpha = 0$ is the model of elastic-perfectly plastic. It is known that, when cross-sectional sizes of members are largely different span-by-span or span lengths are much different span-by-span, the second slope in the story shear-interstory drift relation tends to become larger than 0.1. For this reason, the investigation of larger second stiffness ratios seems important.

From Figs. 10–12, the following findings have been derived.

1) The input velocity level corresponding to $d_{\max}/d_y = 1$ (elastic limit) becomes the largest in the model of $\mathbf{c}_{DI}$ or $\mathbf{c}_{opt,1}$.
2) As the second stiffness ratio after yielding becomes larger, the concentration of plastic deformation to particular stories is hard to occur and the maximum interstory drift distribution becomes smoother especially in the model of $\mathbf{c}_{DI}$.
3) As the second stiffness ratio after yielding becomes larger, the maximum interstory drift increases monotonically with respect to the input velocity level V.
4) The model of elastic-perfectly plastic ($\alpha = 0$) does not necessarily provide the maximum interstory drift.
5) The model of elastic-perfectly plastic ($\alpha = 0$) with $\mathbf{c}_{opt,1}$ sometimes provides larger maximum interstory drifts including plastic deformation than the model with $\mathbf{c}_{opt,2}$, $\mathbf{c}_{opt,3}$.
6) As the second stiffness ratio after yielding becomes larger, the model with $\mathbf{c}_{opt,1}$ exhibits smaller maximum interstory drifts including plastic deformation. This means that, as the model approaches to the linear elastic model, the effectiveness of the damper distribution $\mathbf{c}_{opt,1}$ becomes clear.
7) In the model with $\mathbf{c}_{DI}$, the maximum interstory distribution is not affected so much by the second stiffness ratio after yielding.

It may be concluded that, since $\mathbf{c}_{DI}$ leads to the larger value of the input velocity level corresponding to $d_{\max}/d_y = 1$ (elastic limit) and the smaller maximum interstory drift including plastic deformation, $\mathbf{c}_{DI}$ provides the design with higher robustness (effective for excitation with broader frequency component).

4. Conclusions

The effectiveness of optimal viscous damper placement $\mathbf{c}_{DI}$ for elastic-plastic multi-degree-of-freedom (MDOF) shear building structures under the critical double impulse [1] was demonstrated through the comparison with the optimal damper placement $\mathbf{c}_{opt,1}$, $\mathbf{c}_{opt,2}$, $\mathbf{c}_{opt,3}$ for elastic MDOF structures with respect to the transfer function amplitudes at (1–3)-th natural frequencies. The double impulse is composed of two impulses with opposite directions and the critical interval is determined by using the criterion on the maximum input energy. The critical timing of the second impulse corresponds to the timing which requires the vanishing of the sum of the restoring force and the damping force in the first story. The double impulse pushover (DIP) procedure for determining the input velocity level of the critical double impulse proposed in the previous paper [1] was examined further in this paper to investigate the superiority of $\mathbf{c}_{DI}$ against $\mathbf{c}_{opt,1}$, $\mathbf{c}_{opt,2}$, $\mathbf{c}_{opt,3}$. It was demonstrated that $\mathbf{c}_{DI}$ is more effective than $\mathbf{c}_{opt,1}$, $\mathbf{c}_{opt,2}$, $\mathbf{c}_{opt,3}$ because several higher modes arising in the elastic-plastic response can be well controlled by the design for the double impulse. More detailed results are as follows.

(1) The method for a problem of optimal damper placement with respect to the sum of the transfer function amplitudes at the fundamental natural frequency can be extended straightforwardly to the problem of optimal damper placement with respect to the sum of the transfer function amplitudes at higher-order natural frequencies.
(2) The peak ground acceleration corresponding to $d_{\max}/d_y = 1$ (elastic limit) becomes the largest in the model of $\mathbf{c}_{opt,1}$. The peak ground acceleration corresponding to $d_{\max}/d_y = 1$ in the model of $\mathbf{c}_{DI}$ is also large and is almost equivalent to that in the model of $\mathbf{c}_{opt,1}$. This means sufficient redundancy of $\mathbf{c}_{opt,1}$ and $\mathbf{c}_{DI}$ for elastic limit. As for the plastic deformation after yielding, the model of $\mathbf{c}_{opt,1}$ exhibits larger values than other models in some cases. On the other hand, the model of $\mathbf{c}_{DI}$ exhibits smaller plastic deformations. Also for the models of $\mathbf{c}_{opt,2}$ and $\mathbf{c}_{opt,3}$, the plastic deformation after yielding is apt to become larger.
(3) As the second stiffness ratio after yielding becomes larger, the concentration of plastic deformation to particular stories is hard to occur and the maximum interstory drift distribution becomes smoother especially in the model of $\mathbf{c}_{DI}$.
(4) Since the optimal damper placement $\mathbf{c}_{DI}$ leads to the larger value of the input velocity level corresponding to $d_{\max}/d_y = 1$ (elastic limit) and the smaller maximum interstory drift including plastic deformation, $\mathbf{c}_{DI}$ provides the design with higher robustness (effective for excitation with broader frequency component).

Acknowledgement

Part of the present work is supported by the Grant-in-Aid for Scientific Research (KAKENHI) of Japan Society for the Promotion of Science (No.17K18922, 18H01584) and Sumitomo Rubber Industries, Co. This support is greatly appreciated. In addition, some ground motions used here were recorded by K-NET (National Research Institute for Earth Science and Disaster Resilience in Japan) and JMA (Japan Meteorological Agency).

References

[1] Akehashi H, Takewaki I. Optimal viscous damper placement for elastic-plastic MDOF structures under critical double impulse. Front Built. Environ. 2019;5:20.
[2] Tirca LD, Foti D, Diaferio M. Response of middle-rise steel frames with and without passive dampers to near-field ground motions. Eng Struct 2003;25(2):169–79.
[3] Xu Z, Agrawal AK, He WL, Tan P. Performance of passive energy dissipation systems during near-field ground motion type pulses. Eng Struct 2007;29(2):224–36.
[4] He WL, Agrawal AK. Analytical model of ground motion pulses for the design and assessment of seismic protective systems. *J Struct Eng*, ASCE 2008;134(7):1177–88.
[5] Murakami Y, Noshi K, Fujita K, Tsuji M, Takewaki I. Simultaneous optimal damper placement using oil, hysteretic and inertial mass dampers. Earthquakes Struct 2013;5(3):261–76.

[6] Shiomi T, Fujita K, Tsuji M, Takewaki I. Dual hysteretic damper system effective for broader class of earthquake ground motions. Int. J. Earthquake Impact Eng. 2018;2(3):175–202.
[7] Takewaki I. Building control with passive dampers: -optimal performance-based design for earthquakes-. Singapore: John Wiley & Sons Ltd. (Asia); 2009.
[8] Lagaros ND, editor. Design optimization of active and passive structural control systems. IGI global; 2012.
[9] Domenico DD, Ricciardi G, Takewaki I. Design strategies of viscous dampers for seismic protection of building structures: a review. Soil Dyn Earthq Eng 2019;118:144–65.
[10] Takewaki I. Optimal damper placement for minimum transfer functions. Earthq Eng Struct Dyn 1997;26(11):1113–24.
[11] Aydin E, Boduroglu MH, Guney D. Optimal damper distribution for seismic rehabilitation of planar building structures. Eng Struct 2007;29:176–85.
[12] Fujita K, Yamamoto K, Takewaki I. An evolutionary algorithm for optimal damper placement to minimize interstorey-drift transfer function in shear building. Earthquakes Struct 2010;1(3):289–306.
[13] Adachi F, Yoshitomi S, Tsuji M, Takewaki I. Nonlinear optimal oil damper design in seismically controlled multi-story building frame. Soil Dyn Earthq Eng 2013;44:1–13.
[14] Lavan O, Avishur M. Seismic behavior of viscously damped yielding frames under structural and damping uncertainties. Bull Earthq Eng 2013;11(6):2309–32.
[15] Garcia DL. A simple method for the design of optimal damper configurations in MDOF structures. Earthq Spectra 2001;17:387–98.
[16] Silvestri S, Trombetti T. Physical and numerical approaches for the optimal insertion of seismic viscous dampers in shear-type structures. J Earthq Eng 2007;11:787–828.
[17] Whittle JK, Williams MS, Karavasilis TL, Blakeborough A. A comparison of viscous damper placement methods for improving seismic building design. J Earthq Eng 2012;16(4):540–60.
[18] Cetin H, Aydin E, Ozturk B. Optimal design and distribution of viscous dampers for shear building structures under seismic excitations. Front Built. Environ. 2019;5:90.
[19] Lavan O, Levy R. Optimal design of supplemental viscous dampers for irregular shear-frames in the presence of yielding. Earthq Eng Struct Dyn 2005;34(8):889–907.
[20] Attard TL. Controlling all interstory displacements in highly nonlinear steel buildings using optimal viscous damping. *J Struct Eng*, ASCE 2007;133(9):1331–40.
[21] Lavan O, Cimellaro GP, Reinhorn AM. Noniterative optimization procedure for seismic weakening and damping of inelastic structures. J Struct Eng, ASCE 2008;134(10):1638–48.
[22] Kojima K, Takewaki I. Critical earthquake response of elastic-plastic structures under near-fault ground motions (Part 1: fling-step input). Front Built. Environ. 2015;1:12.
[23] Vamvatsikos D, Cornell CA. Incremental dynamic analysis. Earthq Eng Struct Dyn 2001;31(3):491–514.
[24] Adachi F, Fujita K, Tsuji M, Takewaki I. Importance of interstory velocity on optimal along-height allocation of viscous oil dampers in super high-rise buildings. Eng Struct 2013;56:489–500.
[25] Kojima K, Takewaki I. Critical input and response of elastic-plastic structures under long-duration earthquake ground motions. Front Built. Environ. 2015;1:15.